

# Measurement of $\sigma(e^+e^- \rightarrow \pi^+\pi^-)$ from threshold to 0.85 GeV<sup>2</sup> using Initial State Radiation with the KLOE detector

The KLOE Collaboration

F. Ambrosino<sup>d,e</sup>, F. Archilli<sup>i,j</sup>, P. Beltrame<sup>c,\*,1</sup>, G. Bencivenni<sup>a</sup>,  
 C. Bini<sup>g,h</sup>, C. Bloise<sup>a</sup>, S. Bocchetta<sup>k,ℓ</sup>, F. Bossi<sup>a</sup>,  
 P. Branchini<sup>ℓ</sup>, G. Capon<sup>a</sup>, T. Capussela<sup>a</sup>, F. Ceradini<sup>k,ℓ</sup>,  
 P. Ciambrone<sup>a</sup>, E. De Lucia<sup>a</sup>, A. De Santis<sup>g,h</sup>, P. De Simone<sup>a</sup>,  
 G. De Zorzi<sup>g,h</sup>, A. Denig<sup>c,\*</sup>, A. Di Domenico<sup>g,h</sup>,  
 C. Di Donato<sup>e</sup>, B. Di Micco<sup>k,ℓ</sup>, M. Dreucci<sup>a</sup>, G. Felici<sup>a</sup>,  
 S. Fiore<sup>g,h</sup>, P. Franzini<sup>g,h</sup>, C. Gatti<sup>a</sup>, P. Gauzzi<sup>g,h</sup>,  
 S. Giovannella<sup>a</sup>, E. Graziani<sup>ℓ</sup>, M. Jacewicz<sup>a</sup>, W. Kluge<sup>b</sup>,  
 J. Lee-Franzini<sup>a,m</sup>, D. Leone<sup>b</sup>, P. Massarotti<sup>d,e</sup>, S. Meola<sup>d,e</sup>,  
 S. Miscetti<sup>a</sup>, S. Müller<sup>c,\*,2</sup>, F. Murtas<sup>a</sup>, M. Napolitano<sup>d,e</sup>,  
 F. Nguyen<sup>k,ℓ</sup>, A. Passeri<sup>ℓ</sup>, V. Patera<sup>a,f</sup>, P. Santangelo<sup>a</sup>,  
 C. Taccini<sup>k,ℓ</sup>, L. Tortora<sup>ℓ</sup>, G. Venanzoni<sup>a</sup>, R. Versaci<sup>a,f</sup>

<sup>a</sup>Laboratori Nazionali di Frascati dell'INFN, Frascati, Italy.

<sup>b</sup>Institut für Experimentelle Kernphysik, Universität Karlsruhe, Germany.

<sup>c</sup>Institut für Kernphysik, Johannes Gutenberg - Universität Mainz, Germany.

<sup>d</sup>Dipartimento di Scienze Fisiche dell'Università "Federico II", Napoli, Italy.

<sup>e</sup>INFN Sezione di Napoli, Napoli, Italy.

<sup>f</sup>Dipartimento di Energetica dell'Università "La Sapienza", Roma, Italy.

<sup>g</sup>Dipartimento di Fisica dell'Università "La Sapienza", Roma, Italy.

<sup>h</sup>INFN Sezione di Roma, Roma, Italy.

<sup>i</sup>Dipartimento di Fisica dell'Università "Tor Vergata", Roma, Italy.

<sup>j</sup>INFN Sezione di Roma Tor Vergata, Roma, Italy.

<sup>k</sup>Dipartimento di Fisica dell'Università "Roma Tre", Roma, Italy.

<sup>ℓ</sup>INFN Sezione di Roma Tre, Roma, Italy.

<sup>m</sup>Physics Department, State University of New York at Stony Brook, USA.

## Abstract

We have measured the cross section of the radiative process  $e^+e^- \rightarrow \pi^+\pi^-\gamma$  with the KLOE detector at the Frascati  $\phi$ -factory DAΦNE, from events taken at a CM energy  $W=1$  GeV. Initial state radiation allows us to obtain the cross section for  $e^+e^- \rightarrow \pi^+\pi^-$ , the pion form factor  $|F_\pi|^2$  and the dipion contribution to the muon magnetic moment anomaly,  $\Delta a_\mu^{\pi\pi} = (478.5 \pm 2.0_{\text{stat}} \pm 5.0_{\text{syst}} \pm 4.5_{\text{th}}) \times 10^{-10}$  in the range  $0.1 < M_{\pi\pi}^2 < 0.85$  GeV<sup>2</sup>, where the theoretical error includes a SU(3)  $\chi$ PT estimate of the uncertainty on photon radiation from the final pions. The discrepancy between the Standard Model evaluation of  $a_\mu$  and the value measured by the Muon g-2 collaboration at BNL is confirmed.

*Key words:* Hadronic cross section, initial state radiation, pion form factor, muon anomaly

*PACS:* 13.40.Gp, 13.60.Hb, 13.66.Bc, 13.66.Jn

---

## 1 Introduction

The anomaly of the magnetic moment of the muon,  $a_\mu = (g_\mu - 2)/2$ , is one of the best measured quantities in particle physics [1]. Recent evaluations of the hadronic contributions to the anomaly [2, 3] lead to a discrepancy of about 3 standard deviations of the Standard Model (SM) value from the result of the Brookhaven ( $g_\mu - 2$ ) experiment [1]. A large part of the uncertainty of the theoretical estimate comes from the leading order hadronic contribution  $\Delta a_\mu^{\text{had,lo}}$ , which at low energies is not calculable by perturbative QCD, but can be evaluated via a dispersion relation using measured cross sections of  $e^+e^- \rightarrow \text{hadrons}$  [4]. Initial state radiation (ISR) allows to obtain these cross sections at  $e^+e^-$  colliders operating at fixed energies [5], from the production threshold up to the collision energy. The energy region below 1 GeV, which is accessible with the KLOE experiment at DAΦNE in Frascati, is dominated by the  $\pi^+\pi^-$  channel and contributes  $\sim 75\%$  to the value of  $\Delta a_\mu^{\text{had,lo}}$ , and accounts for  $\sim 40\%$  of its total uncertainty [2]. Better accuracy for the dipion cross section results in an improvement of the SM prediction for  $a_\mu$ .

The KLOE collaboration has already published two measurements of the dipion cross section for  $M_{\pi\pi}^2$  between 0.35 and 0.95 GeV<sup>2</sup> using  $e^+e^- \rightarrow \pi^+\pi^-\gamma$  events from data collected in 2001 [6] and 2002 [7], both at a collision energy  $W=M_\phi$ . We present in the following a new measurement, based on data taken in 2006 at  $W = 1$  GeV, about 20 MeV below the  $\phi$ -meson mass, using different acceptance criteria for the radiated photons. In our previous measurements, the photon was required to be

---

\* Corresponding Authors

*Email addresses:* `beltrame@kph.uni-mainz.de` (P. Beltrame),  
`denig@kph.uni-mainz.de` (A. Denig), `muelers@kph.uni-mainz.de` (S. Müller).

<sup>1</sup> Now at UCLA Physics and Astronomy Dept., Los Angeles, California 90095-1547, USA.

<sup>2</sup> Now at KVI, 9747 AA Groningen, The Netherlands.

emitted at small polar angles ( $\theta < 15^\circ$  or  $\theta > 165^\circ$ ) with respect to the beamline, and therefore escaped detection. In the measurement presented in this Letter, we require the photon to be detected in the electromagnetic calorimeter of KLOE at large polar angles. This allows to extend the  $M_{\pi\pi}^2$  region down to the threshold for the dipion production.

## 2 Measurement of the cross section $e^+e^- \rightarrow \pi^+\pi^-$ at DAΦNE

The KLOE experiment operates at the Frascati  $\phi$ -factory DAΦNE, an  $e^+e^-$ -collider with beams crossing at  $\pi - 0.025$  radians running mainly at a center-of-mass energy  $W \simeq 1020$  MeV, the  $\phi$ -meson mass. The DAΦNE collision energy can be changed only marginally away from the  $\phi$ -resonance energy, and measurements of hadronic cross sections scanning a wider energy range are not possible. However, events with photons radiated by the initial state electron or positron producing a  $\pi^+\pi^-$  pair can cover energies from threshold up to the collision energy. KLOE measures the differential cross section for  $e^+e^- \rightarrow \pi^+\pi^-\gamma$  as a function of the  $\pi^+\pi^-$  invariant mass squared,  $M_{\pi\pi}^2$ , and from this obtains the dipion cross section  $\sigma_{\pi\pi} \equiv \sigma(e^+e^- \rightarrow \pi^+\pi^-)$  according to [8]:

$$\frac{d\sigma(e^+e^- \rightarrow \pi^+\pi^-\gamma)}{dM_{\pi\pi}^2} = \frac{\sigma_{\pi\pi}(M_{\pi\pi}^2)}{s} H(M_{\pi\pi}^2, s) . \quad (1)$$

Eq. 1 defines the dimensionless “radiator function”  $H$ , which can be obtained from QED calculations. Since there is no way to distinguish ISR photons from final state radiation (FSR) photons in the KLOE detector, corrections are necessary and are properly included in the analysis.

The KLOE detector, see Fig. 1, consists of a cylindrical drift chamber [9] surrounded by an electromagnetic calorimeter (EMC) [10]. A superconducting coil provides a magnetic field of 0.52 T along the  $z$ -axis.<sup>3</sup> The drift chamber measures track points with a resolution of  $\sim 0.15$  mm in  $r$ - $\phi$  and  $\sim 2$  mm in  $z$ . The momentum resolution is  $\sigma_{p_t}/p_t \sim 0.4\%$  for tracks with polar angle  $45^\circ < \theta < 135^\circ$ . Energy deposits in the calorimeter close in space and time are combined in “clusters” by the reconstruction program. The cluster energy resolution is  $\sigma_E/E \sim 5.7\%/\sqrt{E}$  (GeV) and the time resolution is  $\sigma_t \sim 54$  ps/ $\sqrt{E}$  (GeV)  $\oplus$  100 ps.

As mentioned above, the previous KLOE measurements [6, 7] used events with photons emitted within cones of  $\theta_\gamma < 15^\circ$  around the beamline (narrow cones in Fig. 1) and two charged pion tracks with  $50^\circ < \theta_\pi < 130^\circ$  (wide cones in Fig. 1). In this configuration, the photon is not detected, its direction is reconstructed from the pion momenta by closing kinematics:  $\vec{p}_\gamma \simeq \vec{p}_{\text{miss}} = -(\vec{p}_{\pi^+} + \vec{p}_{\pi^-})$ . These requirements

<sup>3</sup> The line which bisects the angle between the two colliding beams is taken as the  $z$ -axis of the KLOE coordinate system with incoming positrons going along positive values of  $z$ . The  $x$ -axis is horizontal, pointing to the center of the collider rings, while the  $y$ -axis is vertical, directed upwards.

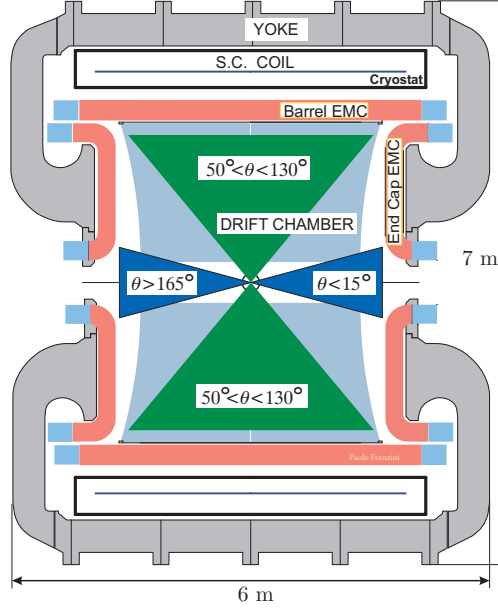


Fig. 1. Vertical cross section in the  $y - z$  plane of the KLOE detector, showing the small and large angle regions for photons and pions used in the different KLOE measurements.

guarantee high statistics for ISR events (because of the divergence of the ISR cross section at small photon angles), and a reduced background contamination (from the resonant process  $e^+e^- \rightarrow \phi \rightarrow \pi^+\pi^-\pi^0$  as well as from the final state radiation process  $e^+e^- \rightarrow \pi^+\pi^-\gamma_{\text{FSR}}$ ). However, requiring the photons at small angles, the low mass dipion region is not reachable since below  $0.35 \text{ GeV}^2$  both pions are emitted at small angles and therefore outside acceptance, resulting in a loss of events.

To reach the dipion threshold, in the new measurement we require events to have a photon detected in the calorimeter at large polar angles,  $50^\circ < \theta_\gamma < 130^\circ$  (wide cones in Fig. 1), the same region where also pion tracks are detected. However, compared to the measurements with photons at small angles, these conditions imply a reduction in statistics of about a factor of 5, and an increase of the background from the process  $\phi \rightarrow \pi^+\pi^-\pi^0$ , as well as the irreducible background from events with final state radiation and from  $\phi$  radiative decays. The hadronic uncertainties associated with the theoretical description of the  $\phi$  radiative decays to the scalar mesons  $f_0(980)$  and  $f_0(600)$  together with the background from the  $\phi \rightarrow \rho\pi \rightarrow (\pi\gamma)\pi$  decay contribute to the uncertainty of the measurement [11]. To reduce the background contamination and the mentioned uncertainties, we collected data at a collision energy of  $W = 1 \text{ GeV}$ ,  $4.5 \Gamma_\phi$  (about 20 MeV) below the  $\phi$ -meson peak, decreasing the  $\phi$ -meson production by about a factor of 80. This reduces the effect of  $f_0\gamma$  and  $\rho\pi$  decays of the  $\phi$ -meson to the level of a few percent.

## 2.1 Event selection

Requirements to select events are:

- (1) A trigger from two energy deposits larger than 50 MeV in two sectors of the

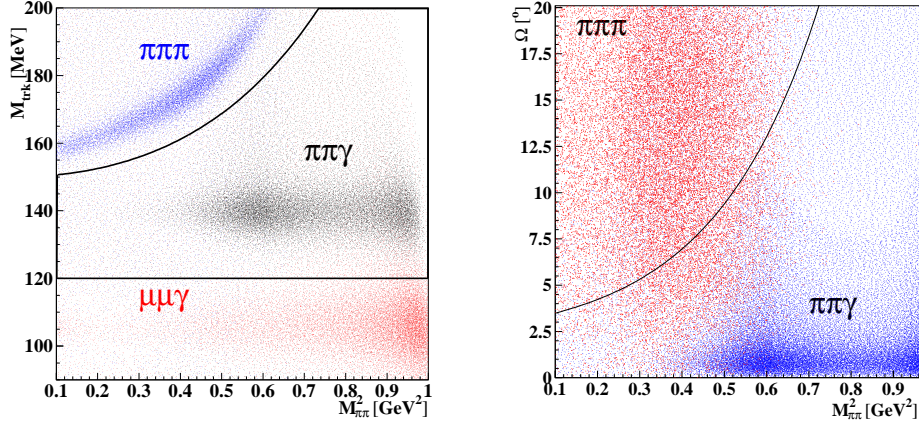


Fig. 2. Left: MC signal and background distributions in the  $M_{\text{trk}}-M_{\pi\pi}^2$  plane. Right: the same, in the  $\Omega-M_{\pi\pi}^2$  plane. Black lines indicate the cuts described in the text.

barrel calorimeter [13].

- (2) A fast offline background filter has to be satisfied [17] to reject machine background and cosmic ray events.
- (3) Two tracks with opposite sign curvature and satisfying  $50^\circ < \theta < 130^\circ$  coming from the interaction point. The latter condition is obtained requiring each track to cross a cylinder centered around the interaction point with 8 cm radius and 14 cm length. Cuts on  $|\vec{p}| > 200$  MeV and  $p_t > 160$  MeV or  $|p_z| > 90$  MeV, respectively, are required to ensure good reconstruction efficiency
- (4) At least one photon with  $50^\circ < \theta_\gamma < 130^\circ$  and  $E_\gamma > 20$  MeV must be detected, where a photon is defined as a cluster in the EMC not associated to a track. If several photons fulfill the criteria, the one with the highest energy is chosen.
- (5) A particle identification variable ( $\pi$ -e PID) is evaluated for each track associated to a cluster in the calorimeter, and an event with both tracks identified as electrons, due to radiative Bhabha scattering events, is rejected.
- (6) The event must satisfy cuts on the track mass variable,  $M_{\text{trk}}$ .<sup>4</sup> Fig. 2, left, shows how a cut in  $M_{\text{trk}} > 120$  MeV rejects  $\mu^+\mu^-\gamma$  events, while a  $M_{\pi\pi}^2$ -dependent cut rejects  $\pi^+\pi^-\pi^0$  events.
- (7)  $\pi^+\pi^-\pi^0$  events are further rejected by a cut on the angle  $\Omega$  between the directions of the detected photon and of the missing momentum  $\vec{p}_{\text{miss}}$ . Fig. 2, right, shows the  $M_{\pi\pi}^2$ -dependent cut used to reject  $\pi^+\pi^-\pi^0$  events situated at large  $\Omega$  values.

About 0.6 million events in the  $M_{\pi\pi}^2$  range between 0.1 and 0.85  $\text{GeV}^2$  are selected.

## 2.2 Determination of the cross section

The radiative differential cross section is obtained subtracting the background count  $N_{\text{bkg}}$  from the observed count  $N_{\text{obs}}$  in bins of  $\Delta M_{\pi\pi}^2 = 0.01$   $\text{GeV}^2$ , and dividing by

<sup>4</sup>  $M_{\text{trk}}$  is computed from the measured momenta of the two particles  $\vec{p}_\pm$  assuming they have the same mass:  $(\sqrt{s} - \sqrt{|\vec{p}_+|^2 + M_{\text{trk}}^2} - \sqrt{|\vec{p}_-|^2 + M_{\text{trk}}^2})^2 - (\vec{p}_+ + \vec{p}_-)^2 = M_\gamma^2 = 0$ .

the selection efficiency,  $\epsilon(M_{\pi\pi}^2)$ , and by the integrated luminosity  $\mathcal{L}$ :

$$\frac{d\sigma_{\pi\pi\gamma}}{dM_{\pi\pi}^2} = \frac{N_{\text{obs}} - N_{\text{bkg}}}{\Delta M_{\pi\pi}^2} \frac{1}{\epsilon(M_{\pi\pi}^2) \mathcal{L}} \quad (2)$$

### 2.2.1 Background subtraction

After selection cuts, residual background events from  $\mu^+\mu^-\gamma$ ,  $\pi^+\pi^-\pi^0$ ,  $e^+e^-\gamma$  and a small fraction of  $\phi \rightarrow K^+K^-$ ,  $\phi \rightarrow \eta\gamma$  events survive. Their number,  $N_{\text{bkg}}$ , is found by fitting the  $M_{\text{trk}}$  spectrum of the selected data sample with a superposition of Monte Carlo (MC) distributions describing signal and background (the  $e^+e^-\gamma$  distribution is obtained from a control sample of data using the  $\pi$ -e PID estimator to select electrons). The fit parameters are the normalization factors for the background distributions, obtained for 15 intervals in  $M_{\pi\pi}^2$  of 0.05 GeV<sup>2</sup> width. The background contamination is dominated by the  $\mu^+\mu^-\gamma$  contribution and is found to be less than 10% above 0.3 GeV<sup>2</sup>, while reaching the level of 50% at the dipion production threshold. Systematic uncertainties of the background estimates are obtained from the errors on the normalization coefficients, yielding values smaller than 0.2% above 0.5 GeV<sup>2</sup>, with a gradual increase to 3.4% at threshold.

We also estimate the contribution from the processes  $e^+e^- \rightarrow \phi \rightarrow (f_0, \sigma)\gamma \rightarrow \pi^+\pi^-\gamma$  and  $e^+e^- \rightarrow \rho^\pm\pi^\mp \rightarrow (\pi^\pm\gamma)\pi^\mp$  to the signal using a modified version of the PHOKHARA MC generator [14]. Despite the fact that the data have been taken with DAΦNE running 20 MeV below the mass of the  $\phi$  meson, an effect of several percent is found, mostly below 0.3 GeV<sup>2</sup>, that needs to be subtracted from the spectrum. Moreover, there is also a sizable non-resonant  $\rho^\pm\pi^\mp$  contribution. The systematic error assigned to this contribution reflects the uncertainty of the production mechanism for these channels. It is negligible above 0.5 GeV<sup>2</sup>, but reaches a value of 6.5% at threshold.

### 2.2.2 Efficiency and systematics evaluation

Efficiencies for the offline background filter, trigger and the  $\pi$ -e PID estimator are obtained from data control samples. All other efficiencies (including geometrical acceptance) are evaluated as one combined *global efficiency* from samples of MC generated events passing the full simulation of the detector response.

Events are generated using the PHOKHARA event generator, which includes next-to-leading order ISR [15] and leading order FSR calculations, as well as simultaneous emission of one ISR and one FSR photon [16]. The generator is interfaced with the KLOE detector simulation code GEANFI [17]. All MC efficiencies are compared to the efficiencies obtained from data control samples, and small corrections are applied to the efficiencies for tracking and photon detection. For all other efficiencies, the MC prediction agrees well with the results from data.

*Offline background filter.* Its efficiency is evaluated from a downsampled control sample retained during the data taking, and is larger than 99%. To overcome statistical limitations of the control sample, a polynomial parametrization is used below



0.4 GeV<sup>2</sup>. The uncertainty of the parameters introduces a systematic error ranging from 0.1 to 0.5%.

*Trigger.* The efficiency is obtained from a subsample of  $\pi^+\pi^-\gamma$  events in which two out of the three particles satisfy the trigger requirements. The trigger response for the third particle is parametrized as a function of its momentum and direction, and the efficiency as a function of  $M_{\pi\pi}^2$  is obtained using kinematic event distributions from MC. It is larger than 99.5%. As a consistency check, the procedure is applied to a sample of  $\pi^+\pi^-\gamma$  events from MC and the outcome is compared to the MC efficiency for an event to satisfy the trigger criteria using the same sample. The fractional difference between the two methods of a few per mill is taken as the systematic uncertainty.

*Pion-electron PID.* The PID estimator is based on time-of-flight and energy and shape of the calorimeter cluster associated to each track. Each track is extrapolated to the calorimeter and at least one cluster is searched for within a sphere of radius  $|\vec{r}_{\text{imp}} - \vec{r}_{\text{clu}}| < 90$  cm around the track impact point,  $\vec{r}_{\text{imp}}$ . The efficiency for each track is evaluated on a clean sample of  $\pi^+\pi^-\gamma$  events from data where one track with an associated cluster is identified to be a pion, and evaluating the probability for the other track to have an associated cluster and also to be recognized as a pion. From this, the event probability to satisfy the selection criteria of having at least one track to be identified as a pion is found. It has been verified to be larger than 99.5% using control samples from data and MC. A similar consistency check as in the trigger efficiency evaluation reveals a maximum uncertainty of a few per mill only below 0.15 GeV<sup>2</sup>.

*Tracking.* This efficiency is contained in the global MC efficiency. Its value is between 97 and 98%. The correction for the difference in data and MC efficiency is obtained comparing the efficiencies for a single pion track as a function of momentum and polar angle from MC and data control samples containing a fully reconstructed pion track of opposite charge and one photon. Event kinematics from MC are then used to get the efficiencies as a function of  $M_{\pi\pi}^2$ . The data efficiency is found to be approximately 0.3% lower than the MC efficiency due to the presence of split tracks not well reproduced in the simulation. The MC-data difference is included as a correction in the analysis. The corresponding systematic uncertainty is estimated varying the radius and length of the cylindrical region around the interaction point the tracks must cross to be selected. It is found to be 0.3%.

*Photon detection.* The photon detection efficiency has been measured using a sample of  $\pi^+\pi^-\pi^0$  events selected from data requiring two oppositely charged tracks and one photon coming from the decay of a  $\pi^0$ . The efficiency is estimated requiring to observe a second photon in a cone around the predicted direction. The efficiency results to be close to 100%, and data and MC efficiencies are in excellent agreement in the energy range of interest. The value from data is few per mill lower only for  $M_{\pi\pi}^2 > 0.8$  GeV<sup>2</sup>. Therefore, the systematic uncertainty is considered negligible.

The efficiencies for the cuts in  $M_{\text{trk}}$  and  $\Omega$  as well as the geometrical acceptance for pions and photon are already included in the global efficiency from MC. Their

systematic uncertainties are obtained as follows:

- The systematic uncertainties due to the  $M_{\text{trk}}$  and  $\Omega$  cuts are obtained by varying the cuts shown in Fig. 2 within reasonable limits of the resolution in  $M_{\text{trk}}$  and  $\Omega$  angle ( $\sigma_{M_{\text{trk}}} \sim 3$  MeV,  $\sigma_{\Omega} \sim 2^\circ$ ) and evaluating the effect on the  $\pi^+\pi^-\gamma$  spectrum. For  $M_{\text{trk}}$ , one obtains an uncertainty that is in the range of 0.1 to 0.4% above 0.5 GeV<sup>2</sup>, whereas below it increases to 3% at threshold. The uncertainty on the  $\Omega$  cuts is negligible above 0.5 GeV<sup>2</sup>, and reaches 1.4% at threshold.
- In a similar way, the systematic effects due to the polar angle requirements for the pions and the detected photon ( $50^\circ < \theta_{\pi,\gamma} < 130^\circ$ ) are estimated by changing the angular acceptance by  $\pm 2^\circ$  for  $\theta_\pi$ , and  $\pm 5^\circ$  for  $\theta_\gamma$ . The resulting uncertainty is about 0.3% above 0.5 GeV<sup>2</sup>. Below, it increases to 1.9% at threshold.

The detector resolution is unfolded using a Bayesian method [18]. The high momentum resolution of the KLOE drift chamber makes this correction small, and as a result the statistical errors for different bins in  $M_{\pi\pi}^2$  become only weakly correlated. Comparison of different unfolding methods gives non-negligible differences only in the two bins close to the  $\rho - \omega$  interference ( $0.60 < M_{\pi\pi}^2 < 0.62$  GeV<sup>2</sup>). The difference of about 2% is taken as a systematic uncertainty for these two bins.

The absolute energy calibration of the KLOE detector is validated with a fit of the pion form factor [27]. The  $\omega$ -meson mass is found to be  $m_\omega = (782.6 \pm 0.3)$  MeV, in excellent agreement with the value from PDG [12].

Parametrized fractional systematic uncertainties as functions of  $M_{\pi\pi}^2$  are given in [27]. Fractional systematic uncertainties which are constant over the range of  $M_{\pi\pi}^2$  covered in this measurement are listed in Table 1.

### 2.2.3 Luminosity and radiative corrections

The absolute normalization of the data sample is performed by counting Bhabha events at large polar angles ( $55^\circ < \theta < 125^\circ$ ). The effective cross section is  $\sigma_{\text{Bhabha}} \simeq 430$  nb. To obtain the integrated luminosity,  $\mathcal{L}$ , the observed number of Bhabha events is divided by the effective cross section evaluated by the Monte Carlo generator Babayaga@NLO [19, 20], which includes QED radiative corrections with the parton shower algorithm, and which has been interfaced with the KLOE detector simulation. The estimated theoretical uncertainty of this generator is 0.1%. The experimental uncertainty on the luminosity measurement is 0.3%, dominated by the systematics on the angular acceptance. The integrated luminosity of the dataset used in the analysis is  $(232.6 \pm 0.2_{\text{th}} \pm 0.7_{\text{exp}})$  pb<sup>-1</sup>, with negligible statistical error. A detailed description of the KLOE luminosity measurement can be found in [21].

The radiator function  $H$  used to extract the cross section  $\sigma_{\pi\pi}$  from the measured differential cross section for  $e^+e^- \rightarrow \pi^+\pi^-\gamma$  in Eq. 1 is obtained from the PHOKHARA MC generator, which includes complete next-to-leading order ISR corrections [22], with a precision of 0.5% mostly due to the effect of missing higher order terms. In addition, the cross section is corrected for the vacuum polarization [23] (running of  $\alpha_{\text{em}}$ ), and the shift between the measured value of  $M_{\pi\pi}^2$  and the squared virtual photon 4-momentum transfer  $q^2 \equiv (M_{\pi\pi}^0)^2$  for events with pions radiating a pho-



ton in the final state. Again the PHOKHARA generator, which includes FSR in the pointlike-pion approximation [24], is used to estimate the second correction: a matrix relating  $M_{\pi\pi}^2$  to  $(M_{\pi\pi}^0)^2$ , giving the probability for an event in a bin of  $M_{\pi\pi}^2$  to originate from some different bin of  $(M_{\pi\pi}^0)^2$ , is used to correct the spectrum.

The validity of the pointlike-pion approach used in the MC generator is compared with a SU(3)  $\chi$ PT calculation [25]. For intermediate and high values of  $M_{\pi\pi}$  no significant disagreement is found, while below the  $\rho$  mass peak region, deviations of up to 7% at the two-pion threshold are found [26]. In absence of more advanced theoretical investigations, we take the  $M_{\pi\pi}$ -dependent difference between the two methods as an estimate of the systematic uncertainty related to the pointlike-pion approach. The entry for “FSR treatment” in Table 1 takes into account this uncertainty, as well as the one due to the limited knowledge of the pion form factor value at  $\sqrt{s} = 1$  GeV.

### 3 Results

The differential  $\pi^+\pi^-\gamma$  cross section is obtained from Eq. 2 performing the analysis as described in Sec. 2.2. The total cross section  $\sigma_{\pi\pi}$  is then computed dividing by the radiator function  $H$ , as described in Eq. 1. To obtain the bare cross section,  $\sigma_{\pi\pi}^{\text{bare}}$ , we remove the effects from vacuum polarization of the virtual photon produced in the  $e^+e^-$  annihilation according to:

$$\sigma_{\pi\pi}^{\text{bare}}(s') = \sigma_{\pi\pi}(s') \times \left( \frac{\alpha(0)}{\alpha(s')} \right)^2, \quad (3)$$

where  $s' \equiv (M_{\pi\pi}^0)^2$  and  $\alpha(0)$  is the fine structure constant in the limit  $q^2 = 0$  ( $\alpha(0) = e^2/4\pi\epsilon_0\hbar c$ ), and  $\alpha(s')$  represents its effective value at  $(M_{\pi\pi}^0)^2$ . We use the parameterization given in [34] for  $\alpha(0)/\alpha(s')$ .

The squared modulus of the pion form factor  $|F_\pi|^2$  is derived from

$$|F_\pi(s')|^2(1 + \eta_{\text{FSR}}(s')) = \frac{3}{\pi} \frac{s'}{\alpha^2 \beta_\pi^3} \sigma_{\pi\pi}(s'), \quad (4)$$

where  $\beta_\pi = \sqrt{1 - 4m_\pi^2/s'}$  is the pion velocity. The factor  $(1 + \eta_{\text{FSR}}(s'))$  describes the effect of FSR assuming pointlike pions (see [28, 29]). In this way, for the radiative corrections applied to  $\sigma_{\pi\pi}^{\text{bare}}$  and  $|F_\pi|^2$ , we adopt the same definition used in energy scan measurements [30–32]:  $\sigma_{\pi\pi}^{\text{bare}}$  is inclusive with respect to final state radiation, and undressed from vacuum polarization effects, while  $|F_\pi|^2$  contains vacuum polarization effects with final state radiation removed.

Our results are summarized in Table 2, which gives

- the observed differential cross section  $d\sigma(e^+e^- \rightarrow \pi^+\pi^-\gamma)/dM_{\pi\pi}^2$  as a function of the measured invariant mass of the dipion system,  $M_{\pi\pi}^2$ , with  $0^\circ < \theta_\pi < 180^\circ$  and at least one photon in the angular region  $50^\circ < \theta_\gamma < 130^\circ$  with  $E_\gamma > 20$  MeV, with statistical and systematic error;

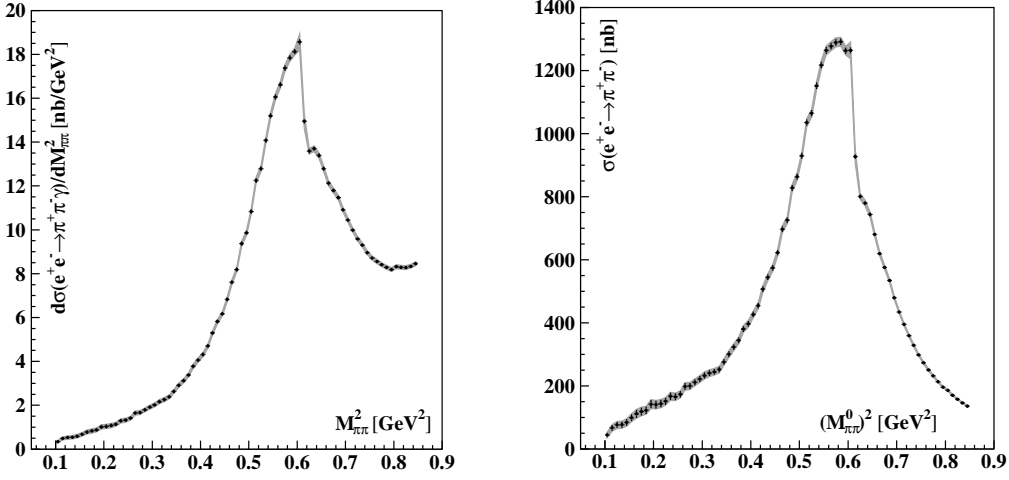


Fig. 3. Left: Differential cross section for  $e^+e^- \rightarrow \pi^+\pi^-\gamma$ , with  $50^\circ < \theta_\gamma < 130^\circ$ . Right: bare cross section  $\sigma_{\pi\pi}^{\text{bare}}$  for  $e^+e^- \rightarrow \pi^+\pi^-$ . Data points have statistical error attached, the gray band gives the statistical and systematic uncertainty (added in quadrature).

- the *bare* cross section  $\sigma^{\text{bare}}(e^+e^- \rightarrow \pi^+\pi^-)$ , inclusive of FSR, but with vacuum polarization effects removed, as a function of  $(M_{\pi\pi}^0)^2$ , with statistical error;
- the squared modulus of the pion form factor, dressed with vacuum polarization, but with FSR effects removed, as a function of  $(M_{\pi\pi}^0)^2$ , with statistical error.

The statistical errors given in Table 2 are weakly correlated as a result of the resolution unfolding. The systematic error for each value of  $M_{\pi\pi}^2$  is obtained combining in quadrature all the individual contributions in each column in Table 1. For the differential cross section for  $e^+e^- \rightarrow \pi^+\pi^-\gamma$ , these systematic errors are reported for convenience in Table 2. Polynomial parameterizations as a function of  $M_{\pi\pi}^2$  can be found in [27] if the contributions listed in Table 1 are not constant in  $M_{\pi\pi}^2$ .

Fig. 3, left, shows the observed differential cross section for  $e^+e^- \rightarrow \pi^+\pi^-\gamma$ , while Fig. 3, right, shows the cross section  $\sigma_{\pi\pi}^{\text{bare}}$ . The latter is the input to the dispersion integral for  $\Delta a_\mu^{\pi\pi}$  [4]:

$$\Delta a_\mu^{\pi\pi} = \frac{1}{4\pi^3} \int_{s_{\min}}^{s_{\max}} ds \sigma_{\pi\pi}^{\text{bare}}(s) K(s), \quad (5)$$

which is computed as the sum of the values for  $\sigma_{\pi\pi}^{\text{bare}}$  listed in Table 2 multiplied by the bin width of 0.01 GeV<sup>2</sup> and the kernel function  $K(s)$ , which behaving approximately like  $1/s$  [35] enhances the contributions at low values of  $s$ . The integration limits are  $s_{\min} = 0.10$  GeV<sup>2</sup> and  $s_{\max} = 0.85$  GeV<sup>2</sup>. Statistical errors of the  $\sigma_{\pi\pi}^{\text{bare}}$  values are summed in quadrature to obtain the statistical error of  $\Delta a_\mu^{\pi\pi}$ . The systematic error of  $\Delta a_\mu^{\pi\pi}$  is obtained as follows: the individual systematic uncertainties of the  $\sigma_{\pi\pi}^{\text{bare}}$  values (listed in Table 1) are added linearly in the summation because they are all fully bin-to-bin correlated. Then the different contributions to the systematic uncertainty of  $\Delta a_\mu^{\pi\pi}$  are added in quadrature to get the total experimental

and theory systematic errors. We find

$$\Delta a_\mu^{\pi\pi}(0.1 - 0.85 \text{ GeV}^2) = (478.5 \pm 2.0_{\text{stat}} \pm 5.0_{\text{exp}} \pm 4.5_{\text{th}}) \times 10^{-10} . \quad (6)$$

The combined fractional systematic error of our value for  $\Delta a_\mu^{\pi\pi}$  is 1.4%.

Data tables and covariance matrices as well as further documentation of the measurement are given in [27].

	$\sigma_{\pi\pi\gamma}$	$\sigma_{\pi\pi}^{\text{bare}}$	$ F_\pi ^2$	$\Delta a_\mu^{\pi\pi}$ (0.1 - 0.85 GeV <sup>2</sup> )
	threshold ; $\rho$ -peak			
Background Filter	0.5% ; 0.1%			negligible
Background subtraction	3.4% ; 0.1%			0.5%
$f_0 + \rho\pi$ bkg.	6.5% ; negl.			0.4%
$\Omega$ cut	1.4% ; negl.			0.2%
Trackmass cut	3.0% ; 0.2%			0.5%
$\pi$ -e PID	0.3% ; negl.			negligible
Trigger	0.3% ; 0.2%			0.2%
Acceptance	1.9% ; 0.3%			0.5%
Unfolding	negl. ; 2.0%			negligible
Tracking	0.3%			
Software Trigger (L3)	0.1%			
Luminosity	0.3%			
Experimental syst.				1.0%
FSR treatment	-	7% ; negl.		0.8%
Radiator function $H$	-	0.5%		
Vacuum Polarization	-	Ref. [34]	-	0.1%
Theory syst.				0.9%

Table 1

Systematic errors on  $\sigma_{\pi\pi\gamma}$ ,  $\sigma_{\pi\pi}^{\text{bare}}$ ,  $|F_\pi|^2$  and  $\Delta a_\mu^{\pi\pi}$ . All errors are fully bin-to-bin correlated. If the error is not constant over the range of  $M_{\pi\pi}^2$ , the value at threshold and at the  $\rho$ -peak (0.6 GeV<sup>2</sup>) is given. The uncertainty on  $\Delta a_\mu^{\pi\pi}$  is composed of a 0.6% contribution coming from the SU(3)  $\chi$ PT calculation and a 0.5% one from the uncertainty of  $|F_\pi|^2$  at  $\sqrt{s} = 1$  GeV. Complete parameterizations of the errors can be found in Ref. [27].

$M_{\pi\pi}^2 (M_{\pi\pi}^0)^2$ GeV <sup>2</sup>	$\sigma_{\pi\pi\gamma}$ nb/GeV <sup>2</sup>	$\sigma_{\pi\pi}^{bare}$ nb	$ F(\pi) ^2$	$M_{\pi\pi}^2 (M_{\pi\pi}^0)^2$ GeV <sup>2</sup>	$\sigma_{\pi\pi\gamma}$ nb/GeV <sup>2</sup>	$\sigma_{\pi\pi}^{bare}$ nb	$ F(\pi) ^2$	$M_{\pi\pi}^2 (M_{\pi\pi}^0)^2$ GeV <sup>2</sup>	$\sigma_{\pi\pi\gamma}$ nb/GeV <sup>2</sup>	$\sigma_{\pi\pi}^{bare}$ nb	$ F(\pi) ^2$
0.105	0.34±0.06±0.03	44±7	1.63±0.27	0.355	2.91±0.09±0.03	301±9	7.13±0.22	0.605	18.57±0.12±0.35	1264±10	43.42±0.33
0.115	0.49±0.06±0.03	67±9	1.92±0.26	0.365	3.12±0.09±0.04	323±9	7.79±0.22	0.615	14.95±0.11±0.34	927±7	34.09±0.27
0.125	0.53±0.07±0.03	76±9	1.89±0.24	0.375	3.38±0.09±0.03	344±9	8.43±0.22	0.625	13.59±0.10±0.08	801±7	29.81±0.25
0.135	0.54±0.07±0.03	77±10	1.74±0.23	0.385	3.78±0.09±0.04	381±9	9.47±0.23	0.635	13.70±0.10±0.08	779±6	29.08±0.24
0.145	0.59±0.08±0.04	84±11	1.78±0.23	0.395	4.06±0.09±0.04	397±9	10.02±0.23	0.645	13.38±0.10±0.08	743±6	27.91±0.23
0.155	0.67±0.08±0.04	99±11	2.02±0.23	0.405	4.32±0.09±0.04	426±9	10.94±0.23	0.655	12.79±0.10±0.07	680±6	25.77±0.21
0.165	0.78±0.09±0.03	111±13	2.21±0.26	0.415	4.70±0.09±0.04	454±9	11.83±0.23	0.665	12.13±0.09±0.07	619±5	23.68±0.20
0.175	0.83±0.09±0.03	119±12	2.32±0.24	0.425	5.29±0.09±0.04	507±9	13.40±0.24	0.675	11.79±0.09±0.07	576±5	22.25±0.19
0.185	0.88±0.08±0.03	122±12	2.38±0.23	0.435	5.82±0.09±0.05	545±9	14.62±0.24	0.685	11.47±0.09±0.07	534±5	20.84±0.18
0.195	1.01±0.09±0.03	142±13	2.75±0.26	0.445	6.17±0.09±0.04	574±9	15.64±0.24	0.695	10.91±0.09±0.07	479±4	18.91±0.16
0.205	1.04±0.09±0.03	140±13	2.72±0.24	0.455	6.83±0.09±0.05	622±9	17.21±0.25	0.705	10.45±0.08±0.06	434±4	17.32±0.15
0.215	1.07±0.09±0.03	144±12	2.81±0.23	0.465	7.61±0.10±0.05	697±9	19.55±0.26	0.715	9.98±0.08±0.06	394.9±3.4	15.92±0.14
0.225	1.14±0.09±0.03	151±11	2.97±0.22	0.475	8.19±0.10±0.05	725±9	20.64±0.26	0.725	9.58±0.08±0.06	359.4±3.2	14.64±0.13
0.235	1.29±0.09±0.03	167±12	3.31±0.23	0.485	9.37±0.10±0.06	828±10	23.90±0.28	0.735	9.30±0.08±0.06	328.5±3.0	13.53±0.12
0.245	1.32±0.09±0.03	165±11	3.32±0.22	0.495	9.86±0.10±0.06	863±10	25.30±0.28	0.745	8.96±0.08±0.06	298.2±2.7	12.42±0.11
0.255	1.41±0.08±0.03	173±10	3.52±0.21	0.505	10.84±0.11±0.07	930±10	27.65±0.29	0.755	8.71±0.07±0.05	272.9±2.4	11.49±0.10
0.265	1.64±0.09±0.03	198±11	4.10±0.22	0.515	12.25±0.11±0.08	1035±10	31.24±0.31	0.765	8.55±0.07±0.05	250.6±2.2	10.67±0.09
0.275	1.67±0.08±0.03	199±10	4.18±0.21	0.525	12.79±0.11±0.08	1065±10	32.64±0.31	0.775	8.42±0.07±0.05	231.8±2.1	9.97±0.09
0.285	1.79±0.08±0.03	211±10	4.49±0.21	0.535	14.08±0.12±0.09	1151±10	35.84±0.33	0.785	8.29±0.07±0.05	213.2±1.9	9.27±0.08
0.295	1.92±0.08±0.03	222±10	4.78±0.21	0.545	15.20±0.12±0.09	1217±11	38.49±0.34	0.795	8.19±0.07±0.05	196.1±1.8	8.62±0.08
0.305	2.02±0.09±0.03	233±10	5.10±0.21	0.555	16.06±0.12±0.09	1264±11	40.59±0.34	0.805	8.32±0.07±0.05	185.2±1.6	8.23±0.07
0.315	2.17±0.09±0.03	241±9	5.36±0.21	0.565	16.62±0.12±0.10	1278±10	41.68±0.34	0.815	8.29±0.07±0.05	170.2±1.5	7.64±0.07
0.325	2.26±0.09±0.03	244±9	5.53±0.21	0.575	17.38±0.12±0.10	1289±10	42.71±0.34	0.825	8.28±0.07±0.05	157.4±1.4	7.13±0.06
0.335	2.38±0.09±0.03	252±9	5.79±0.21	0.585	17.85±0.12±0.10	1291±10	43.38±0.34	0.835	8.34±0.07±0.05	146.1±1.2	6.69±0.06
0.345	2.63±0.09±0.04	276±9	6.44±0.21	0.595	18.13±0.12±0.10	1263±10	42.94±0.33	0.845	8.45±0.07±0.05	135.9±1.1	6.28±0.05

Table 2

Cross sections  $\sigma_{\pi\pi\gamma}$ ,  $\sigma_{\pi\pi}^{bare}$  and pion form factor  $|F_\pi|^2$  in bins of 0.01 GeV<sup>2</sup>. The squared mass values are given at the bin center. The  $\sigma_{\pi\pi\gamma}$  cross section is given as a function of  $M_{\pi\pi}^2$ . The  $\sigma_{\pi\pi}^{bare}$  cross section and  $|F_\pi|^2$  are given as function of  $(M_{\pi\pi}^0)^2$ , see text. The error given is the statistical uncertainty. For  $\sigma_{\pi\pi\gamma}$ , the second error gives the total systematic uncertainty.

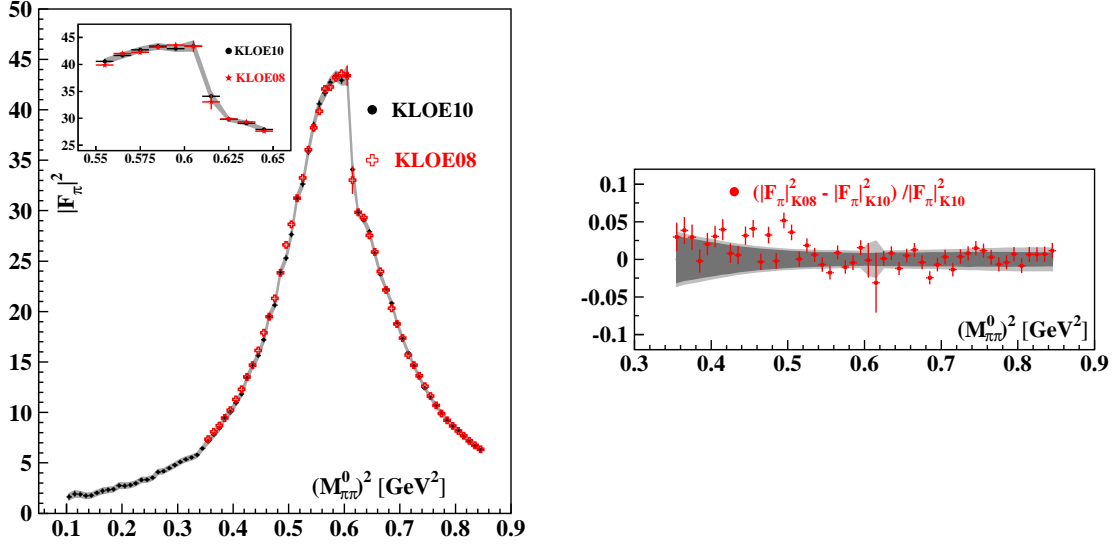


Fig. 4. Comparison of the present result, KLOE10, with the previous KLOE result, KLOE08 [7]. Left: Pion form factor  $|F_\pi|^2$ . Right: Fractional difference between KLOE08 and KLOE10 results. The dark (light) gray band gives the statistical (total) error for the present result. Errors on KLOE08 points contain the combined statistical and systematic uncertainty.

#### 4 Comparison with previous KLOE results

We compare in Fig. 4 our present result for the pion form factor in the range of  $0.35 < (M_{\pi\pi}^0)^2 < 0.85 \text{ GeV}^2$  with the result of the previous KLOE measurement [7]. We stress that data sets have been obtained at different operating conditions of the DAΦNE collider, and different selection cuts in acceptance were used. Also the analysis procedures are different since in the previous KLOE analysis the radiated photon was not detected. An excellent agreement is found for  $(M_{\pi\pi}^0)^2 > 0.5 \text{ GeV}^2$ , while below the new result is lower by few percent. This is reflected also in the evaluation of the dispersion integral, see Eq. 5, between 0.35 and  $0.85 \text{ GeV}^2$ . The new result gives a value of  $\Delta a_\mu^{\pi\pi}$  which is lower by  $(0.8 \pm 0.9)\%$  (see Table 3). The experimental systematic precision in the overlapping range of  $(M_{\pi\pi}^0)^2$  is comparable in both measurements. Systematic effects are independent in the two cases except for the uncertainties related to the radiator function, the vacuum polarization and the luminosity measurement, which are identical.

	$\Delta a_\mu^{\pi\pi}(0.35 - 0.85 \text{ GeV}^2) \times 10^{-10}$
KLOE10 (This work)	$376.6 \pm 0.9_{\text{stat}} \pm 2.4_{\text{exp}} \pm 2.3_{\text{th}}$
KLOE08 [7]	$379.6 \pm 0.4_{\text{stat}} \pm 2.4_{\text{exp}} \pm 2.2_{\text{th}}$

Table 3

$\Delta a_\mu^{\pi\pi}$  values in the range  $0.35 - 0.85 \text{ GeV}^2$ .

Constructing the weighted average of the two measurements we evaluate the dispersion integral from 0.1 to  $0.95 \text{ GeV}^2$ , using the method of [33]. Separating out

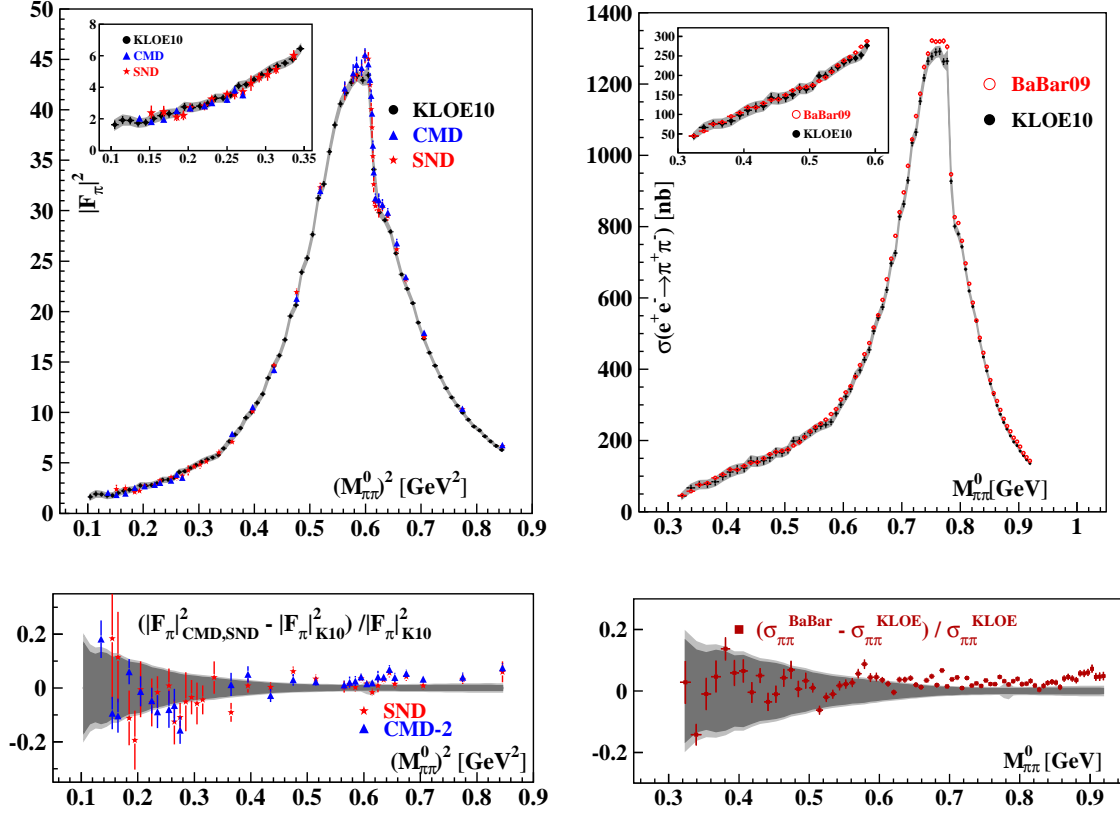


Fig. 5. Top left:  $|F_\pi|^2$  from CMD-2 [30, 31], SND [32] and the present KLOE result as function of  $(M_{\pi\pi}^0)^2$ . Bottom left: Fractional difference between CMD-2 or SND and KLOE. Top right:  $\sigma_{\pi\pi}^{\text{bare}}$  from BaBar [36] and the new KLOE result as function of  $M_{\pi\pi}^0$ . Bottom right: Fractional difference between BaBar and KLOE. CMD-2, SND and BaBar data points have the total uncertainty attached. The dark (light) band in the lower plots shows statistical (total) error of the KLOE result.

the uncertainties common to both measurements, we obtain

$$\Delta a_\mu^{\pi\pi}(0.1 - 0.95 \text{ GeV}^2) = (488.6 \pm 5.3_{\text{indep.}} \pm 2.9_{\text{common}}) \times 10^{-10}. \quad (7)$$

The combined fractional total error of  $\Delta a_\mu^{\pi\pi}$  in this range is 1.2%.

## 5 Comparison with results from the CMD-2, SND and BaBar experiments

In Fig. 5, the new KLOE result is compared with the results from the energy scan experiments CMD-2 [30, 31] and SND [32] in Novosibirsk and the result obtained from the BaBar experiment at SLAC [36], which uses the ISR method. Whenever several data points fall in one KLOE bin of 0.01  $\text{GeV}^2$ , the values are statistically averaged. Fig. 5, left, shows the comparison of  $|F_\pi|^2$  obtained by the CMD-2 and SND collaborations with the present KLOE result. On the  $\rho$ -peak and above, the agreement with the SND result is rather good, while the result from the CMD-2 collaboration is slightly higher than the new KLOE measurement, confirming the



observation already reported in the previous KLOE publication [7]. Below the  $\rho$ -peak, all three experiments are in agreement within uncertainties. Fig. 5, right, shows the present KLOE and the BaBar result for the bare cross section as a function of  $M_{\pi\pi}^0$ . The fractional difference between BaBar and KLOE results is shown together with the statistical and total fractional KLOE errors. The two results are in agreement within errors below 0.65 GeV, while above the new BaBar measurement is about 2-3% higher.

## 6 Conclusions

We have measured the differential radiative cross section  $d\sigma(e^+e^- \rightarrow \pi^+\pi^-\gamma)/dM_{\pi\pi}^2$  in the interval  $0.1 < M_{\pi\pi}^2 < 0.85 \text{ GeV}^2$  using  $230 \text{ pb}^{-1}$  of data obtained while the DAΦNE  $e^+e^-$  collider was running at  $W \simeq 1 \text{ GeV}$ , 20 MeV below the  $\phi$ -meson peak. A systematic uncertainty of 1% has been reached above  $0.4 \text{ GeV}^2$ , rising up to 10% when approaching  $0.1 \text{ GeV}^2$ . This increase is mainly due to the uncertainty in the production mechanism of  $\phi$  radiative decays and the uncertainty on the treatment of final state radiation.

From this measurement, we have extracted the squared modulus of the pion form factor in the time-like region,  $|F_\pi|^2$ , and the bare cross section for the process  $e^+e^- \rightarrow \pi^+\pi^-$ ,  $\sigma_{\pi\pi}^{\text{bare}}$ , in intervals of  $0.01 \text{ GeV}^2$  of  $(M_{\pi\pi}^0)^2$ , the squared mass of the virtual photon produced in the  $e^+e^-$ -collision after the radiation of a hard photon in the initial state. Our new measurement is in good agreement with previous KLOE measurements, and reaches down to the dipion production threshold. A reasonable agreement has also been found with the results from the Novosibirsk experiments CMD-2 and SND, especially at low values of  $(M_{\pi\pi}^0)^2$ . Comparing our result with the new result from the BaBar collaboration, we have found agreement within errors below  $0.4 \text{ GeV}^2$ , while above the BaBar result is higher by 2-3%.

Evaluating the dispersion integral for the dipion contribution to the muon magnetic moment anomaly,  $\Delta a_\mu^{\pi\pi}$ , in the range between 0.1 and  $0.85 \text{ GeV}^2$  we have found

$$\Delta a_\mu^{\pi\pi}(0.1 - 0.85 \text{ GeV}^2) = (478.5 \pm 2.0_{\text{stat}} \pm 5.0_{\text{exp}} \pm 4.5_{\text{th}}) \times 10^{-10},$$

confirming the discrepancy between the SM evaluation for  $a_\mu$  and the experimental value measured by the Muon g-2 collaboration at BNL.

Combining our result with the previous KLOE results, we have calculated  $\Delta a_\mu^{\pi\pi}$  in the range  $0.1 < M_{\pi\pi}^2 < 0.95 \text{ GeV}^2$  obtaining

$$\Delta a_\mu^{\pi\pi}(0.1 - 0.95 \text{ GeV}^2) = (488.6 \pm 6.0) \times 10^{-10}.$$

The KLOE experiment covers  $\sim 70\%$  of the leading order hadronic contribution to the muon anomaly with  $\sim 1\%$  total error.

## Acknowledgements

We wish to acknowledge the work of B. Valeriani in the development of the  $\pi$ -e PID estimator. We would like to thank Carlo Michel Carloni Calame, Henryk Czyż, Fred Jegerlehner, Johann Kühn, Guido Montagna, Germán Rodrigo, Olga Shekhovtsova, Thomas Teubner and Sergiy Ivashyn for numerous useful discussions.

We thank the DAΦNE team for their efforts in maintaining low background running conditions and their collaboration during all data-taking. We want to thank our technical staff: G.F. Fortugno and F. Sborzacchi for their dedicated work to ensure an efficient operation of the KLOE computing facilities; M. Anelli for his continuous support to the gas system and the safety of the detector; A. Balla, M. Gatta, G. Corradi and G. Papalino for the maintenance of the electronics; M. Santoni, G. Paoluzzi and R. Rosellini for the general support to the detector; C. Piscitelli for his help during major maintenance periods. This work was supported in part by EURODAPHNE, contract FMRX-CT98-0169; by the German Federal Ministry of Education and Research (BMBF) contract 06-KA-957; by the German Research Foundation (DFG), 'Emmy Noether Programme', contracts DE839/1-4; and by the EU Integrated Infrastructure Initiative HadronPhysics Project under contract number RII3-CT-2004-506078.

## References

- [1] G. W. Bennett *et al.* [Muon G-2 Collaboration], Phys. Rev. D **73** (2006) 072003.  
For a review see J. P. Miller, E. de Rafael, B. Lee Roberts, Rep. Prog. Phys. **70** (2007) 795.
- [2] F. Jegerlehner and A. Nyffeler, Phys. Rept. **477** (2009) 1.
- [3] M. Davier, A. Hoecker, B. Malaescu, C. Z. Yuan and Z. Zhang, Eur. Phys. J. C **66** (2010) 1
- [4] C. Bouchiat and L. Michel, J. Phys. Radium **22** (1961) 121.
- [5] S. Actis *et al.*, Eur. Phys. J. C **66** (2010) 585.
- [6] A. Aloisio *et al.* [KLOE Coll.], Phys. Lett. B **606** (2005) 12.
- [7] F. Ambrosino *et al.* [KLOE Coll.], Phys. Lett. B **670** (2009) 285.
- [8] S. Binner, J. H. Kühn and K. Melnikov, Phys. Lett. B **459** (1999) 279.
- [9] M. Adinolfi *et al.*, Nucl. Instrum. Meth. A **488** (2002) 51.
- [10] M. Adinolfi *et al.*, Nucl. Instrum. Meth. A **482** (2002) 364.
- [11] F. Ambrosino *et al.* [KLOE Collaboration], Phys. Lett. B **634** (2006) 148.
- [12] C. Amsler *et al.* [Particle Data Group], Phys. Lett. B **667** (2008) 1.
- [13] M. Adinolfi *et al.*, Nucl. Instrum. Meth. A **492** (2002) 134.

- [14] O. Shekhovtsova, <http://ific.uv.es/~rodrigo/phokhara/>, PHOKHARA6.1, unpublished (2008).
- [15] G. Rodrigo, H. Czyż, J. H. Kühn and M. Szopa, *Eur. Phys. J. C* **24** (2002) 71.
- [16] H. Czyż, A. Grzelinska, J. H. Kühn and G. Rodrigo, *Eur. Phys. J. C* **33** (2004) 333.
- [17] F. Ambrosino *et al.*, *Nucl. Instrum. Meth. A* **534** (2004) 403.
- [18] G. D’Agostini, *Nucl. Instrum. Meth. A* **362** (1995) 487.
- [19] C. M. Carloni Calame *et al.*, *Nucl. Phys. B* **584** (2000) 459.
- [20] G. Balossini *et al.*, *Nucl. Phys. B* **758** (2006) 227.
- [21] F. Ambrosino *et al.* [KLOE Collaboration], *Eur. Phys. J. C* **47** (2006) 589.
- [22] H. Czyż, A. Grzełińska, J. Kühn, G. Rodrigo, *Eur. Phys. J. C* **27** (2003) 563.
- [23] F. Jegerlehner, *Nucl. Phys. Proc. Suppl.* **162** (2006) 22.
- [24] H. Czyż, A. Grzełińska, J. Kühn, *Phys. Lett. B* **611** (2005) 116.
- [25] T. Fuchs, B. Pasquini, C. Unkmeir and S. Scherer, *Czech. J. Phys.* **52** (2002) B135.
- [26] S. Ivashyn, H. Czyz and A. Korchin, *Acta Phys. Polon. B* **40** (2009) 3185.
- [27] Data tables and covariance matrices:  
<http://www.lnf.infn.it/kloe/ppg>.
- [28] J.S. Schwinger, “Particles, Sources, and Fields. VOL. 3”, *Redwood City, USA: ADDISON-WESLEY (1989) 318 P. (Advanced Book Classics Series)*.
- [29] F. Jegerlehner, *Nucl. Phys. Proc. Suppl.* **162** (2006) 22.
- [30] R. R. Akhmetshin *et al.* [CMD-2 Coll.], *Phys. Lett. B* **648** (2007) 28.
- [31] R. R. Akhmetshin *et al.* [CMD-2 Coll.], *JETP Lett.* **84** (2006) 413.
- [32] M. N. Achasov *et al.* [SND Coll.], *J. Exp. Theor. Phys.* **103** (2006) 380.
- [33] S. I. Eidelman and F. Jegerlehner, *Z. Phys. C* **67** (1995) 585.
- [34]  $\alpha(s)$  values kindly provided by Fred Jegerlehner,  
<http://www-com.physik.hu-berlin.de/~fjeger/alphaQEDn.uu> (2003).
- [35] B. E. Lautrup and E. de Rafael, *Phys. Rev.* **174** (1968) 1835.
- [36] B. Aubert *et al.* [BABAR Collaboration], *Phys. Rev. Lett.* **103** (2009) 231801.